Robust Aeroelastic Tailoring For Composite Aircraft Wings

Muhammad F. Othman[a,1,*], Jonathan E. Cooper[a,2], Alberto Pirrera[a,3], Paul M. Weaver[a,4], Gustavo H.C. Silva[b,5]

[a] *Advanced Composites Centre for Innovation and Science, Aerospace Engineering Department, University of Bristol, Queens Building, University Walk, Bristol BS8 1TR, UK*
[b] *Embraer S.A., São José dos Campos, São Paulo, 12227-901, Brazil*

Abstract

An optimisation framework is presented for robust design configuration of composite aircraft wings through consideration of uncertainties in material properties, ply orientations and thickness. A detailed Finite Element wing box model of a regional jet airliner is used as a benchmark. The wing structure is optimised for minimum weight with strain, buckling, flutter/divergence and gust constraints. Polynomial Chaos Expansion approach is used to efficiently quantify the effects of uncertainty in the design parameters. This method is used to determine the probability of flutter/divergence occurring, and the allowable root bending moment being exceeded, for any given design specification which is then optimised using a Particle Swarm Optimisation algorithm. Results are compared with deterministic solution for optimal flutter speed and minimum root bending moment. Three layup strategies were undertaken, a first which only consists of 0°, ±45° and 90° plies, a second which included ±30° and ±60° plies and a third which also uses ±15° and ±75° plies. A minimum improvement in reliability of 32.6% is achieved for laminate with 0°, ±45° and 90° plies and highest reduction in mean root bending moment value is obtained with inclusion of ±30° and ±60° plies. The layup strategy with 0°, ±30°, ±45°, ±60° and 90° plies give the optimal robust solution for both flutter and root bending moment responses.

Keywords: *Composite structures, Aeroelastic Tailoring, Multi-constraint optimisation, Robust optimisation, Polynomial Chaos Expansion, Flutter, Gust alleviation, Lamination parameters*

1. Introduction

There is currently a lot of interest in the use of composite materials for aircraft structural design. Although the possibility of aeroelastic tailoring has been around since the early 1980s, most applications of carbon fibre reinforced polymer (CFRP) have been "black metal" designs which do not exploit the anisotropic properties. One possible reason for the delays in designing aeroelastically tailored aircraft structures is the explosion in the number of design variables that occur.

Aeroelastic tailoring is defined as the process of embodiment of the directional stiffness on the wing structure in order to control the aerodynamic deformation, both static and dynamic [1]. The aim for aeroelastic tailoring is to obtain minimum structural weight with improvement in aeroelastic and structural performance of the wing. This can be achieved by modifying the design of bending and torsional coupling of the composite structure by means of material tailoring or structural tailoring.

Recent works on aeroelastic tailoring of composite wings have focused on the optimisation of the wing structure subjected to multiple constraints including stress [2, 3], strain [4], buckling [5], aeroelastic response [2, 6, 7, 8, 9], gust alleviation [7, 4] and aileron effectiveness [5]. Weight minimisation is solely the main objective in aeroelastic tailoring. Weight saving was able to be achieved without compromising the performance contraints of the wing. Other works on aeroelastic tailoring have been focused on multi-level optimisation of the composite wing [10, 4, 8]. Because of high computational costs involved when dealing with detailed finite element models, multi-level or multi-stage optimisation approaches provide a good alternative for aeroelastic tailoring. Multi-

*Corresponding author
Email address: muhammad.othman@bristol.ac.uk (Muhammad F. Othman)
[1] PhD Student.
[2] RAEng Airbus Sir George White Professor of Aerospace Engineering. AFAIAA.
[3] Lecturer in Aerospace Engineering.
[4] Professor in Lightweight Structures.
[5] Tehnology Development Engineer.

level optimisation provides a platform for possibility of improving computational efficiency by reducing the number of design variables required from one level to another as well as to separate different types of analysis within each level.

A further consideration in aeroelastic tailoring is the effect of uncertainty on the entire design process which could be used to develop robust optimum designs. Uncertainty is defined as *"an imperfect state of knowledge or a variability resulting from a variety of factors including, but not limited to, lack of knowledge, applicability of information, physical variation, randomness or stochastic behavior, indeterminacy, judgment, and approximation"* [11]. *"Uncertainty can arise as a result of incomplete information, errors in both analysis and design models, and the uncertain nature of inputs and system parameters"* [12]. Uncertainty in aeroelasticity and composite structure can exist due to a number of sources including nonlinearity of the structure, errors in aerodynamic prediction, variability in material properties such as material non-homogeneity, fibre misalignment, waviness, wrinkling and defects, as well as the manufacturing tolerance and thickness variations [13, 14].

There are a number of methods available to address uncertainties in composite structures including Monte Carlo Simulation (MCS) [15, 16], Polynomial Chaos Expansion (PCE) [14, 17, 13, 18] and Stochastic Collocation [19]. MCS is a common and straightforward technique used to quantify uncertainties. However, large computational efforts are necessary to produce meaningful results. MCS and perturbation technique methods have been used to model flutter behavior of an aeroelastic wing with uncertain bending and torsional stiffness [20]. PCE has been used to model uncertainties in a number of models, such as a composite lifting surface with uncertain material properties, fiber direction angles and ply thickness [14], and aeroelastic stability of composite plate wings with uncertain ply orientations using lamination parameters [13]. Ref. [13] reported on the uncertainties quantification for aeroelastic stability using simple cantilever wing model representation.

Polynomial Chaos Expansion (PCE) together with lamination parameters are used for the analysis which resulted in greater computational efficiency as compared to other approaches such as Monte Carlo Simulation. The inclusion of uncertainty studies in aeroelastic models would be significant in order to quantify and identify a robust composite wing design which is insensitive to small changes in design parameters, such as ply orientations material properties and thicknesses.

In this paper, an attempt was made to perform robust optimisation on a detailed finite element wing box model for minimum structural weight with multiple constraints including strain, buckling, aeroelastic response and gust alleviation. The Polynomial Chaos Expansion (PCE) model is used to quantify the variation in material properties, ply angles and ply thicknesses of a composite material. Three layup strategies are adopted as design variables for robust optimisation to account for ply angle variations in the model.

2. Model Definition

A detailed Finite Element (FE) wing box model of a regional jet airliner was used for the analysis to demonstrate the effectiveness of the method. A swept wing configuration with aspect ratio of 10 is taken as the case study. The wing geometry and the load carrying wing box within the planform are depicted in Fig. 1(a). The dimension given is in normalised form. The structural entities including the spars, ribs and stringers sections were defined in the model. Three main spars and the ribs, including those at the root and tip are modelled and positioned equidistant in the spanwise direction aligned with the global x-axis. The stringers are included in the model as bar elements. The skin, ribs and spars are defined using composite material properties while others using mass less aluminium properties.

A total of 25, 543 elements with bars and shells representation are used for the structural mesh. Both, the aerodynamic grids and the structural mesh of the composite wing model are coupled together using a surface spline which is used to interpolate the aerodynamic grid points to the structural mesh points for aeroelastic analysis. For aerodynamic modelling, the aerodynamic panels are divided into two sections, with the outer wing having a higher mesh density as compared to the inner wing section as shown in Fig. 1(b).

3. Deterministic Optimisation

The composite wing structure was optimised for minimum structural weight with strain, buckling, flutter/divergence and gust response constraints. MSc. Nastran was used throughout the analysis. Only the top skin, bottom skin and the spar sections of the wing were optimised because of their effective influence to the wing structure‘s strength and stiffness. A total of 41 panels are modelled for the skin and spar sections as shown in Fig. 2. A penalty function with weighting factors was assigned on the flutter/divergence and gust response constraints. It is very likely that if the wing is optimised considering only one of the parameter, the performance of the other constraints will be poor.

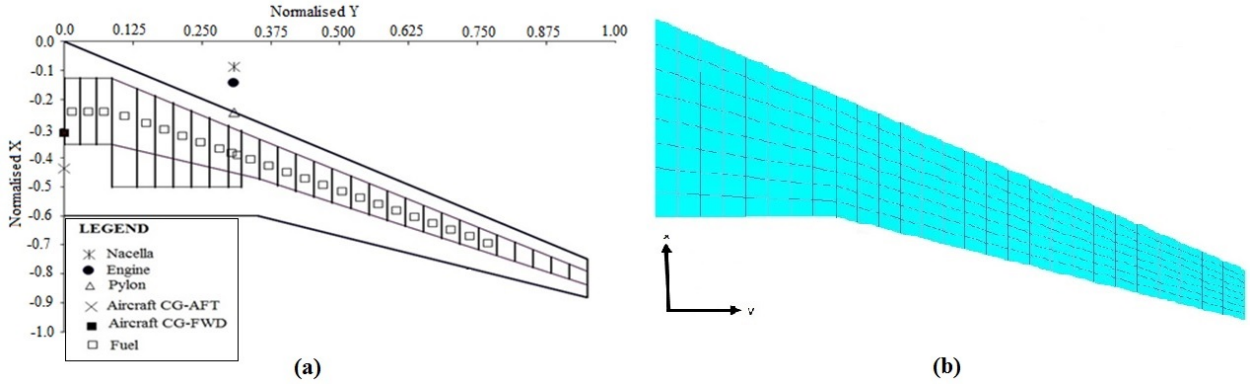

Figure 1: (a) Wing geometry and different mass entities in the FE model, (b) Aerodynamic grid.

Thus, the penalty function introduced should provide an indication of how much the responses have an effect on the optimal solution and is given by following equation.

$$\Omega_{\text{Penalty}} = (w_f \times \frac{V_f - V_{f,\text{Design}}}{V_{f,\text{Design}}})... + (w_g \times \frac{RBM - RBM_{\text{Design}}}{RBM_{\text{Design}}}) \quad (1)$$

where V_f and $V_{f,\text{Design}}$ is the flutter speed and design flutter speed. RBM is the wing root bending moment.

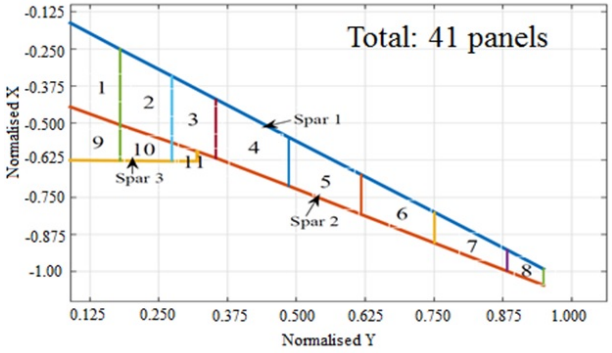

Figure 2: Panel partitions used for the wing model.

For a minimum structural weight optimisation, the strain constraint is defined in terms of Failure Index, FI, using the maximum strain criterion according to Eqn. (3). A static maneuver load case is considered for the analysis, with Mach number, cruise altitude and acceleration of 0.82, 10 000 m and 2.5 g, respectively. The static load for the flight condition is obtained from aerostatic analysis. The upper boundary for strain Failure Index is set as 1.0. For buckling analysis, only the first ten buckling modes were considered with the lower boundary of critical load factor, λ is set as 1.0. In flutter analysis, the upper boundary set as $1.15V_D$, where V_D is the flight dive velocity. The constraint for gust response is set as the minimum value of wing root bending moment (RBM). Explanations for the flutter and gust response analysis are given in detail in Sections 3.2 and 3.3. The multi-constraints optimisation problem for a minimum weight objective is expressed as follows.

$$\begin{cases} \textit{Min. Weight, W(X)} \\ \textit{Strain Failure Index, FI(X)} \leq 1 \quad \textit{(Max. Strain)} \\ \textit{Buckling critical load factor,} \lambda \geq 1 \\ \textit{Flutter speed,} V_f \geq 1.15 V_D \quad (V_D = \textit{Design DIVE speed}) \\ \textit{Wing Root Bending Moment, } RBM = \textit{min(RBM)} \\ \textit{Design Variables,} X = [\xi_1, ..., \xi_4, \xi_9, ..., \xi_{11} \\ \qquad \textit{and} \quad t_{\text{panel},1}, ..., t_{\text{panel},41}] \end{cases} \quad (2)$$

The failure index for the strain constraints is derived from the principal and shear strains as:

$$FI = \frac{\epsilon_L}{\epsilon_{1,\text{allowable}}} \quad \textit{and} \quad \frac{\gamma_{LT}}{\gamma_{LT,\text{allowable}}} \quad (3)$$

where, ϵ_L is the strain in longitudinal direction and γ_{LT} is the shear strain in the longitudinal and transverse directions. The allowable strain values used for the analysis are given in Table 8.

Table 1: Strain allowable values for composite laminate.

Label	Values	Remarks
StrPmin	-5.90E-03	Principal strain under compression
StrPmax	7.10E-03	Principal strain under tension
StrShrmax	4.50E-03	Maximum shear strain
StrShrmin	-4.50E-03	Minimum shear strain

For the deterministic optimisation, a total of 328 design variables were defined in the optimisation problem with seven lamination parameters $(\xi_1, \xi_2, \xi_3, \xi_4, \xi_9, \xi_{10}, \xi_{11})$ and a panel thickness parameter for each of the 41 panels. The deterministic optimisation is performed using the Particle Swarm Optimisation (PSO) algorithm with maximum iteration numbers of 50 and 20 particles for each iteration.

3.1. Composite Material Properties: Lamination Parameters

In classical lamination theory [21], the in-plane (A) and out-of-plane stiffnesses (D) can be described as

$$\begin{Bmatrix} N \\ M \end{Bmatrix} = \begin{Bmatrix} A & 0 \\ 0 & D \end{Bmatrix} \begin{Bmatrix} \epsilon \\ \kappa \end{Bmatrix} \tag{4}$$

where the generalised stress components are $N = \{N_x, N_y, N_{xy}\}^T$ and $M = \{M_x, M_y, M_{xy}\}^T$. The generalised strain components are given by $\epsilon = \{\epsilon_x, \epsilon_y, \epsilon_{xy}\}^T$ and $\kappa = \{\kappa_x, \kappa_y, \kappa_{xy}\}^T$. The in-plane and out-of-plane stiffnesses are given by A_{ij} and D_{ij}, respectively where $i, j = 1, 2, ...6$. The stiffness components, A_{ij} and D_{ij} can be represented by using the stiffness invariants $U_i (i = 1, 2, 3, 4, 5)$ and the in-plane and out-of-plane lamination parameters $\xi_i (i = 1, 2, 3, 4, 9, 10, 11, 12)$ in accordance with the following equation

$$\begin{Bmatrix} A_{11} \\ A_{12} \\ A_{22} \\ A_{66} \\ A_{16} \\ A_{26} \end{Bmatrix} = t \begin{bmatrix} 1 & \xi_1 & \xi_2 & 0 & 0 \\ 0 & 0 & -\xi_2 & 1 & 0 \\ 1 & -\xi_1 & \xi_2 & 0 & 0 \\ 0 & 0 & -\xi_2 & 0 & 1 \\ 0 & \frac{\xi_3}{2} & \xi_4 & 0 & 0 \\ 0 & \frac{\xi_3}{2} & -\xi_4 & 0 & 0 \end{bmatrix} \begin{Bmatrix} U_1 \\ U_2 \\ U_3 \\ U_4 \\ U_5 \end{Bmatrix} \tag{5}$$

$$\begin{Bmatrix} D_{11} \\ D_{12} \\ D_{22} \\ D_{66} \\ D_{16} \\ D_{26} \end{Bmatrix} = \frac{t^3}{12} \begin{bmatrix} 1 & \xi_9 & \xi_{10} & 0 & 0 \\ 0 & 0 & -\xi_{10} & 1 & 0 \\ 1 & -\xi_9 & \xi_{10} & 0 & 0 \\ 0 & 0 & -\xi_{10} & 0 & 1 \\ 0 & \frac{\xi_{11}}{2} & \xi_{12} & 0 & 0 \\ 0 & \frac{\xi_{11}}{2} & -\xi_{12} & 0 & 0 \end{bmatrix} \begin{Bmatrix} U_1 \\ U_2 \\ U_3 \\ U_4 \\ U_5 \end{Bmatrix} \tag{6}$$

where t is the thickness of the plate. By defining the non-dimensional though thickness coordinate denoted by $u(= \frac{2z}{t})$, the lamination parameters can be expressed in terms of ply orientation θ as

$$\{\xi_1, \xi_2, \xi_3, \xi_4\} = \frac{1}{2} \int_{-1}^{1} \{\cos 2\theta(u), \cos 4\theta(u), ... \sin 2\theta(u), \sin 4\theta(u)\} du \tag{7}$$

$$\{\xi_9, \xi_{10}, \xi_{11}, \xi_{12}\} = \frac{3}{2} \int_{-1}^{1} \{\cos 2\theta(u), \cos 4\theta(u), ... \sin 2\theta(u), \sin 4\theta(u)\} u^2 du \tag{8}$$

The lamination parameters are not independent and the relation of the lamination parameters can be expressed in Eqn.(9), which defines the feasible region for the parameters [22].

$$2\xi_1^2 < \xi_2 \tag{9a}$$

$$\xi_9^2 + \xi_{11}^2 \leq 1 \tag{9b}$$

$$2(1 + \xi_{10})\xi_{11}^2 - 4\xi_9\xi_{11}\xi_{12} + \xi_{12}^2 ... -(\xi_{10} - 2\xi_9^2 + 1)(1 - \xi_{10}) \leqslant 0 \tag{9c}$$

For example, the feasible region of (ξ_9, ξ_{10}) when $D_{16} = D_{26} = 0$, i.e. $(\xi_{11}, \xi_{12}) = (0, 0)$, can be expressed from Eqn.(9) by following inequality expression:

$$2\xi_9^2 - 1 \leqslant \xi_{10} \leqslant 1 \tag{10}$$

The use of lamination parameters for the optimisation of composite structures should reduce the numbers of linear equations to approximately determine the feasible region and hence requires less computational efforts in optimisation processes. For balanced symmetric laminates, the stiffness component in $B_{ij} = 0$ and hence the value of ξ_5 to ξ_8 is assumed as zero and ξ_{12}=0. Consequently, only seven variables of lamination parameter were considered as design variables with an additional variable for laminate thickness. The composite material properties are summarised in Table 2.

Table 2: Composite material properties (IM7 tape)[23].

Property	Values
E_1 (GPa)	148.0
E_2 (GPa)	10.3
G_{12} (GPa)	5.90
υ_{12}	0.27
Density, ρ(kgm^{-3})	1580
Ply thickness, t_{ply} (mm)	0.183

3.2. Aeroelastic analysis

In aeroelastic analysis, the flutter/divergence analysis of the composite wing model was performed on MSc Nastran using Sol. 145: Flutter analysis. The PK method was used to predict the flutter/divergence occurrence. The governing equation for the PK method can be described as follows [24].

$$[-M_{hh}p^2 + (B_{hh} - 0.25\rho cV Q_{hh}^I(M,k)/k) + ... (K_{hh} - 0.5\rho V^2 Q_{hh}^R(M,k))]\{u_h\} = 0 \tag{11}$$

where M_{hh} is the modal mass, B_{hh} is the damping, K_{hh} is the stiffness matrix, M, k and u_h are the Mach number, reduced frequency and modal amplitude vector. Q_{hh}^I and Q_{hh}^R are the imaginary and real part of the eigenvalues, Q_{hh}. The flutter/divergence frequencies and damping are obtained from the analysis as functions of velocity and relative model amplitudes. The corresponding critical flutter speed and divergence speeds can be determined via $V - g$ and $V - f$

plots. A total of six modes were assumed for the composite wing model. The instability occurs when the real part of Q_{hh} is positive. The flutter point was determined when the imaginary part of the eigenvalue is non-zero and divergence occurs when the imaginary part of the eigenvalue is zero. The flutter point can be deduced from a $V-g$ plot when the damping equals to zero.

3.3. Gust response

Optimisation of a composite wing for gust load alleviation has been explored by various researchers [4, 25, 26, 16]. Guo et al. [4] considered wing gust response in term of vertical wing tip displacement with time domain. Atmospheric turbulence idealised as discrete gusts or continuous turbulence is one of the critical criteria for aircraft design as specified by aeronautical authorities (CS-25) [27]. A $'1-cosine'$ discrete gust model is governed by the following expression.

$$w_g(t) = \frac{w_{g0}}{2}(1 - cos\frac{2\pi V}{L_g}t) \tag{12}$$

where, w_{g0} is the peak or design gust velocity, L_g is the gust length and V is the flight speed. The gust length, L_g varies from $18m$ to $216m$. For this work, the design gust velocity, w_{g0} is $20ms^{-1}$ and the flight speed,V is $253ms^{-1}$. The gust response constraint for the deterministic optimisation was evaluated in term of minimum strain energy which is governed by wing root bending moment (RBM) against discrete gust load [14, 16]. The aeroelastic dynamic response (Sol. 146) in MSc. Nastran was used to evaluate the discrete gust response for the wing model. The response to a discrete gust was determined by using direct and inverse Fourier transform methods [28]. Only critical gust length was considered for this work which is defined as the maximum absolute value of the root bending moment response.

4. Robust Optimisation

The robust optimisation for the wing structure was performed by considering the variation in material properties, ply angle and ply thickness, t_{ply} of the composite material. The longitudinal, E_1, and the transverse in-plane Young's modulus, E_2 were assumed as the random variables with coefficient of variation = 0.1. The mean and standard deviation for the random variables are given in Table 3. The Polynomial Chaos Expansion (PCE) method was used for stochastic modelling in uncertainties quantification analysis due to computational efficiency. A comparison with Monte Carlo Simulation results was performed to study the accuracy of the PCE model. In order to account for ply angle variation in robust optimisation, three different layup strategies are adopted as design variables for robust analysis together with the uncertainties parameters.

Table 3: Mean and standard deviation values for random variables of the uncertainties parameters.

	E_1 (GPa)	E_2 (GPa)	Ply thickness, t_{ply} (m)
Mean, μ	148.0	10.3	1.83E-04
Std Dev. σ	14.8	1.03	1.83E-06

4.1. Polynomial Chaos Expansion (PCE)

Polynomial Chaos Expansion (PCE) has been used to describe irregularities due to uncertainty in aeroelastic models [17, 13]. The Weiner-Askey Chaos expansion from Askey Scheme [18, 29] can be used to model variation for random variables. The continuous random variables can be modelled using different types of polynomials described in [13]. A simple definition of PCE for any second-order random process $u(\theta)$ can be represented by the expression:

$$\begin{aligned} u(\theta) = a_0\Gamma_0 + \sum_{1}^{\infty} a_{i1}\Gamma_1(\zeta_{i1}(\theta)) + ... \\ \sum_{i1=1}^{\infty}\sum_{i2=1}^{i1} a_{i1i1}\Gamma_2[\zeta_{i1}(\theta),\zeta_{i2}(\theta)] + ... \\ \sum_{i1=1}^{\infty}\sum_{i2=1}^{i1}\sum_{i3=1}^{i2} a_{i1i2i3}\Gamma_3[\zeta_{i1}(\theta),\zeta_{i2}(\theta),\zeta_{i3}(\theta)] + ... \end{aligned} \tag{13}$$

where $\{\zeta_{i1}(\theta)\}_1^{\infty}$ is a set of independent random variables, $\Gamma_p[\zeta_{i1}(\theta),...,\zeta_{ip}(\theta)]$ is the polynomial chaos of order p which composed of multidimensional orthogonal polynomials, $a_{i1},...,a_{ip}$ are the deterministic expansion coefficient and θ is the random character of the quantity involved. If $\{\zeta_{i1}(\theta)\}_1^{\infty}$ is a set of standard Gaussian random variables, the Γ_p terms can be expressed as multi-dimensional Hermite polynomials given by [29]

$$\Gamma_p[\zeta_{i1}(\theta),...,\zeta_{ip}(\theta)] = (-1)^n \frac{\partial^n e^{-\frac{1}{2}\zeta^T\zeta}}{\partial\zeta_{i1}(\theta),...,\partial\zeta_{ip}(\theta)} e^{\frac{1}{2}\zeta^T\zeta} \tag{14}$$

Eqn. 14 is often written as

$$u(\theta) = \sum_{i=0}^{\infty}\beta_i\psi_i(\zeta(\theta)) \tag{15}$$

where there is a one-to-one correlation between $\Gamma_p[\zeta_{i1}(\theta),...,\zeta_{ip}(\theta)]$ and $\psi_i(\zeta(\theta))$ and between β_i and $a_{i1},...,a_{ip}$. In practice, Eqn. 13 is truncated to dimension d of random variable ζ and the highest order (p) of the polynomial. The total number of expansion

coefficients $(P+1)$ is given by

$$P+1=\frac{(d+p)!}{d!p!} \tag{16}$$

The polynomial basis, ψ_i of Hermite-chaos forms a complete orthogonal basis such that

$$\psi_i(\zeta)\psi_j(\zeta)=\int \psi_i(\zeta)\psi_j(\zeta)W(\zeta)d\zeta=\psi_i^2\delta_{ij} \tag{17}$$

where,

$$\delta_{ij}=\begin{cases}0 & \text{if } i\neq j\\ 1 & \text{if } i\neq j\end{cases} \tag{18}$$

and $W(\zeta)$ is the weighting function for the polynomial

$$W(\zeta)=\frac{1}{\sqrt{(2\pi)^n}}e^{-\frac{1}{2}\zeta^T\zeta} \tag{19}$$

The complete basis polynomials are Hermite polynomials in terms of Gaussian variables and are orthogonal with respect to the weighting function $W(\zeta)$. To demonstrate, provided that the input random variables are Gaussian continuous random variables, multivariate polynomial basis is deduced by taking the tensor product of 1-D Hermite polynomials which correspond to each variable. For example, a 2-D expansion of a 3^{rd} order PCE model for a two-dimensional Gaussian input, $\zeta=\{\zeta_1,\zeta_2\}^T$, can be written as

$$\begin{aligned}u_{3^{rd}}=&\beta_0+\beta_1\zeta_1+\beta_2\zeta_2+\beta_3(\zeta_1^2-1)+...\\ &\beta_4\zeta_1\zeta_2+\beta_5(\zeta_2^2-1)+\beta_6(\zeta_1^3-3\zeta_1)+...\\ &\beta_7(\zeta_1^2\zeta_2-\zeta_2)+\beta_8(\zeta_2^2\zeta_1-\zeta_1)+...\\ &\beta_9(\zeta_2^3-3\zeta_2)\end{aligned} \tag{20}$$

where the β_i terms are the unknown coefficients that have to be calculated using a computed test data set.

Fig.3 shows an overview of the PCE process to determine the Probability Density Function (PDF) response of the wing model for Gaussian continuous random variables input. The Latin Hypercube Sampling (LHS) technique [30] was employed to ensure that all test cases of the input variables were selected with equal probability and hence a relatively few number of cases can be chosen and be capable to achieve small response variances at low computational costs. In this work, the material properties (E_1 and E_2) and the ply thickness (t_{ply}) are chosen as the uncertainty parameters. The input random variables are then computed into the FE model together with other lamination parameters (based on layup strategies) and the laminate thickness. A least-squares linear regression model is used together with LHS technique as proposed in [30] to determine the expansion coefficient, β_i.

For example, the sample outputs of the aeroelastic responses (i.e. instability speed, $V_{crit}(\zeta)$), are determined at each sample point, $\zeta_1,...,\zeta_N$ and the response, V_{crit} at each sample point can be presented as N simultaneous equations derived from Eqn. (15).

$$\begin{Bmatrix}V_{crit}(\zeta_1)\\ \vdots\\ V_{crit}(\zeta_N)\end{Bmatrix}=\begin{Bmatrix}\psi_0(\zeta_1) & \cdots & \psi_P(\zeta_1)\\ \vdots & \ddots & \vdots\\ \psi_0(\zeta_N) & \cdots & \psi_P(\zeta_N)\end{Bmatrix}\begin{bmatrix}\beta_1\\ \vdots\\ \beta_P\end{bmatrix}+\begin{bmatrix}\varepsilon_1\\ \vdots\\ \varepsilon_N\end{bmatrix} \tag{21}$$

or in simplified matrix form

$$\{V_{crit}\}=[\psi]\{\beta\}+\{\varepsilon\} \tag{22}$$

where ε is the error associated with simplifying the expansion. The expansion coefficient can be deduced by minimising the error such that:

$$Error,\varepsilon=Min(\sum_{i=1}^{N}\varepsilon_i^2) \tag{23}$$

and

$$\{\beta\}=(\psi^T\psi)^{-1}\psi^T\{V_{crit}\} \tag{24}$$

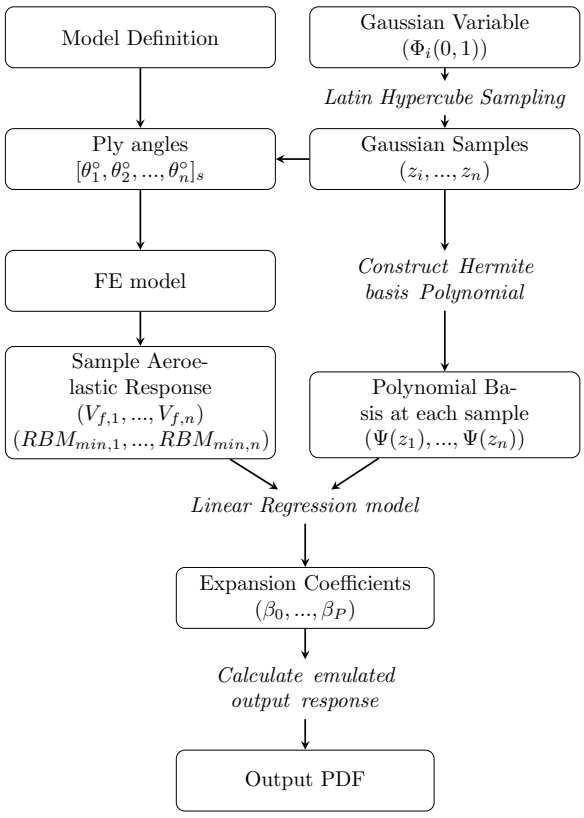

Figure 3: Overview of modelling process using PCE

Once the expansion coefficients are evaluated, they can be used in Eqn.(22) to emulate the response based upon any given combination of uncertainty parameters and predict statistical properties such as mean value, the standard deviation and the probability density function of any output responses at low computational cost.

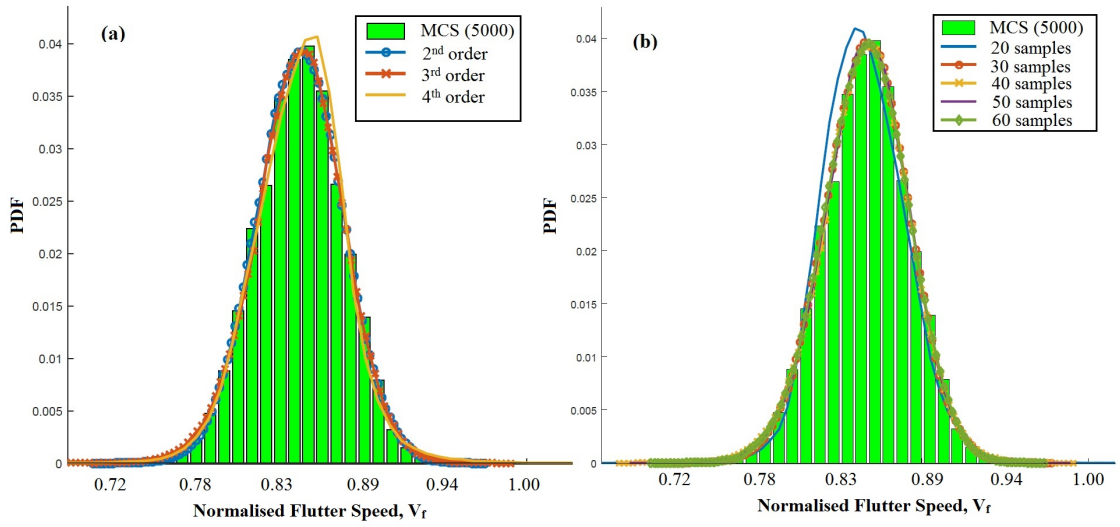

Figure 4: PDF plots for flutter response(a) Different order of PCE model and MCS data, (b) Different number of samples using 3^{rd} order PCE.

The convergence study was performed for the PCE model and compared with MCS results with 5000 simulations. Figs.4(a) and 4(b) show the PDF plots for flutter response at different orders of PCE and different numbers of samples (3^{rd} order PCE) as compared to MCS results. It can be seen that there is an excellent agreement with the MCS data for 1^{st}, 2^{nd} and 3^{rd} order PCE with 30 samples. However, the 4^{th} order shows little discrepancy as compared to MCS data due to the limited number of samples. The study on different numbers of samples for a 3^{rd} order PCE model shows the results starting to converge at number of samples = 30. Hence, it can be remarked that the PCE model can provide an efficient tool for uncertainties quantification with less computational cost. The robust optimisation on this work was performed using a 3^{rd} order PCE model with 30 samples.

4.2. Probabilistic Optimisation

The efficiency of PCE model to emulate the flutter and gust response of the composite wing was utilised for the robust design optimisation with uncertainties consideration. A strategy is adopted where the aeroelastic instability (flutter/divergence) occurrence at design instability speed is minimised. Here, the concept of maximising the reliability of the structure is used in terms of probability of survival such that the instability not occur before a certain design instability speed.

The equivalent strategy was applied for gust response except aiming to maximise the probability of occurence at design root bending moment (RBM) or to increase the area under the PDF plot at design value. Here, three layup strategies were adopted for the design variables of robust optimisation. Only 0°, ±45° and 90° plies are considered in the first layup strategy. In second layup strategy, ±30° and ±60° plies are included to account for extra design spaces for optimisation.

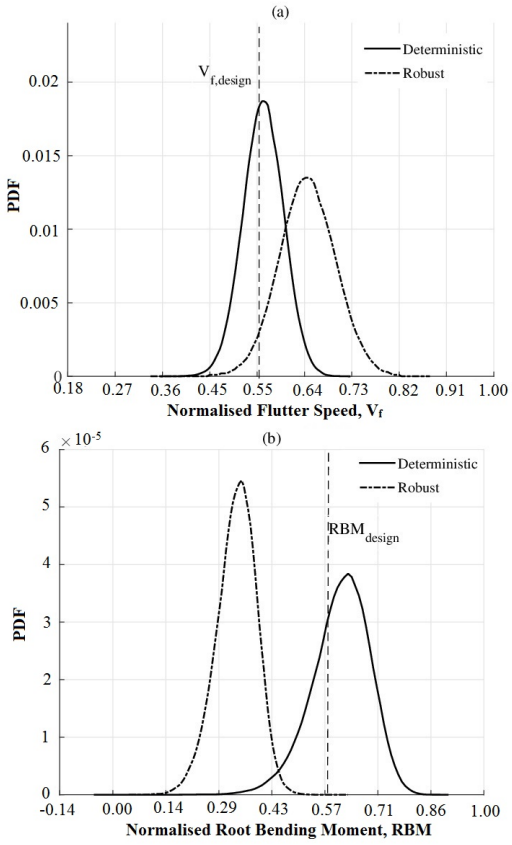

Figure 5: (a) PDF plot for flutter/divergence response, (b) PDF plot for wing root bending moment (RBM).

The additional ±15° and ±75° plies are also included in the third layup strategy. Ply contiguity constraint was applied to ensure no more than four plies of a given orientation are used. For robust optimisation, the deterministic optimal solution is first obtained with the uncertainty parameters. The probability of failure at design values are obtained and further minimised to obtain a robust design configuration. Again, particle swarm optimisation (PSO) was used for the optimisation with 50 iterations and 20 particles.

5. Results and discussion

5.1. Benchmark model

Based on the initial design analysis performed on the benchmark model, the FE results show that the normalised maximum strain is 0.4109 as shown in Fig.8. Higher strain distributions are observed at the junction of inboard and outboard wing, which are caused by geometry change and higher stress concentration. The maximum failure index, FI for strain is 0.3308. The minimum value for critical load factor for the first ten buckling modes is 2.878.

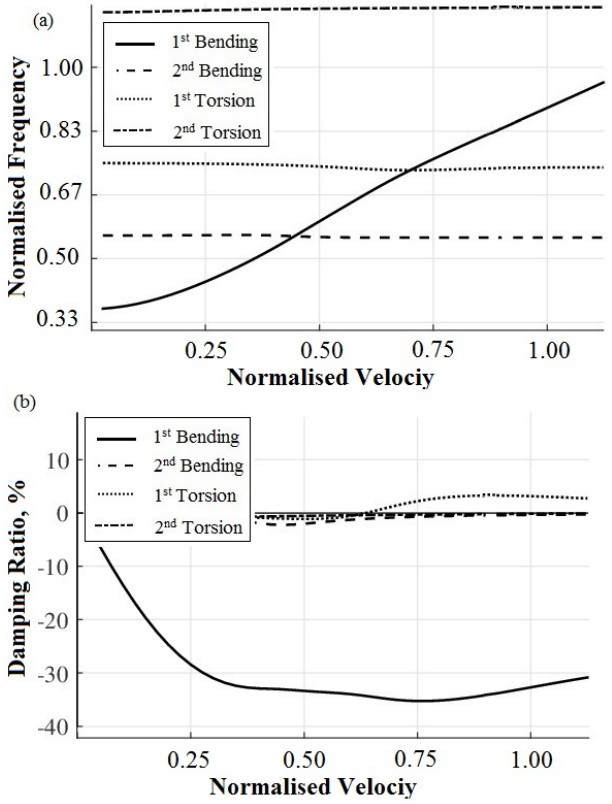

Figure 6: Flutter results for the benchmark model: (a) *V-f* plot; (b) *V-g* plot

The mode shape analysis was performed on the benchmark wing model to determine the critical vibration mode. The first four vibration modes and the normalised frequency of the wing are first bending (0.3683), second bending (0.5605), first torsion (0.7495) and second torsion (1.1438), respectively.

The flutter analysis results are shown in Fig.6 in the form of *V-f* and *V-g* plots using PK method. The results indicate that the first bending mode coupled with the torsion mode is the most critical one, where the normalised flutter speed of 0.6355 at normalised frequency of 0.75 was obtained when the damping reaches zero. The flutter speed obtained is much higher that the normalised design flutter speed of 0.3261. The gust response for the wing is measured in term of wing root bending moment (RBM). The critical value is obtained at gust length of 216 m with normalised RBM value of 4.171. The thickness variation for the skin and spar section of the wing is presented in Fig.7 with normalised structural weight of 0.6122. The results show that the benchmark model has potential for weight saving by aeroelastic tailoring due to an ample safety margin.

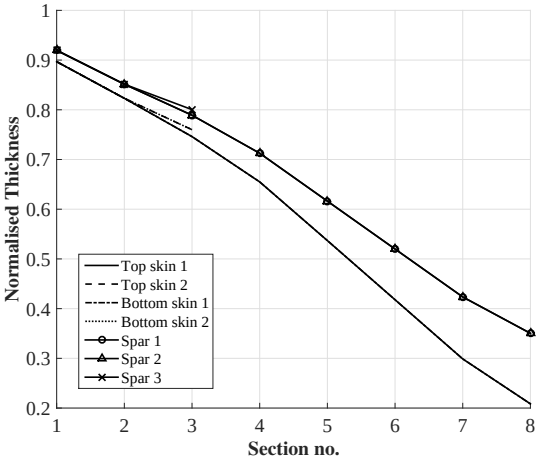

Figure 7: Thickness variation for benchmark model.

5.2. Deterministic model

The normalised structural weight of the wing structure was reduced to 0.5428 which is a 11.3% reduction as compared to the benchmark wing. The minimum weight was obtained after 20 iterations using Particle Swarm optimisation (PSO) with 20 particles as shown in Fig.9.

The thickness variation of the skin and spar section are presented in Fig.10. It is noticed that thickest section is obtained at the kink area of the bottom skin panel where the stress concentration was higher due to engine and pylon mass. A lower thickness value is obtained at the tip of the top skin panel. Although in practice it would be more useful to include the ply drop consideration for manufacturing compatibility, the results shown here provided a reasonable thickness variation for the wing model.

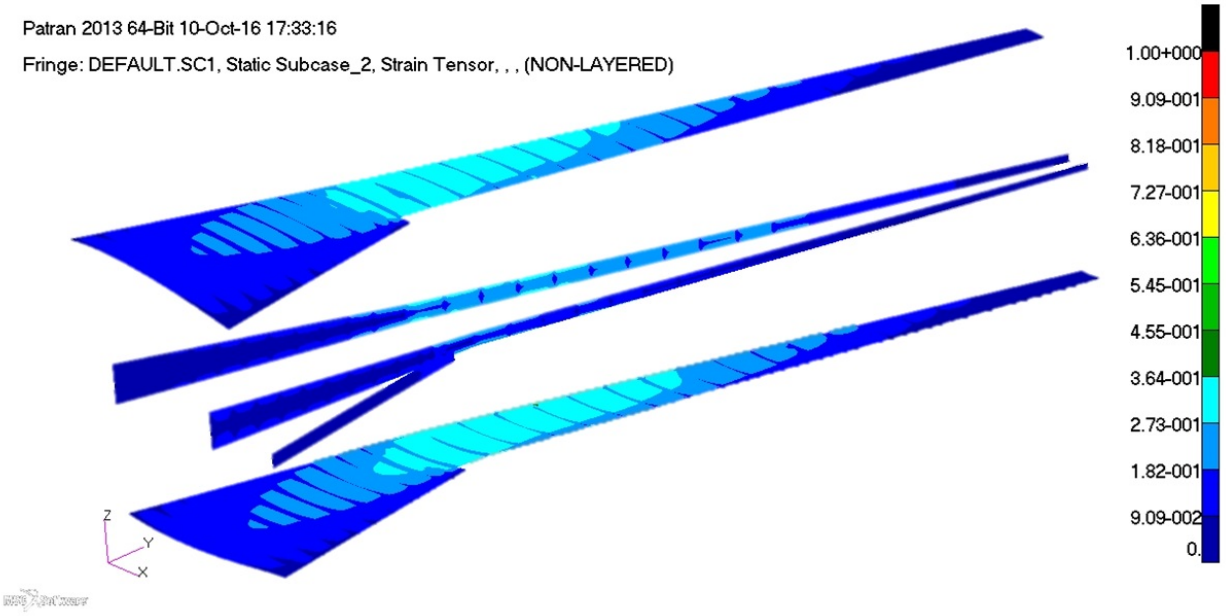

Figure 8: Normalised strain distribution on the benchmark wing model.

The normalised maximum strain value increased to 1 with the maximum failure index, FI of 0.76. A higher strain concentration was observed at the leading edge close to the junction of inboard and outboard wing. However, it is also noticed that the strains are distributed uniformly from the root to 3/4 of the wing span as compared to the benchmark wing. This is caused by a thicker panel section obtained at this section.

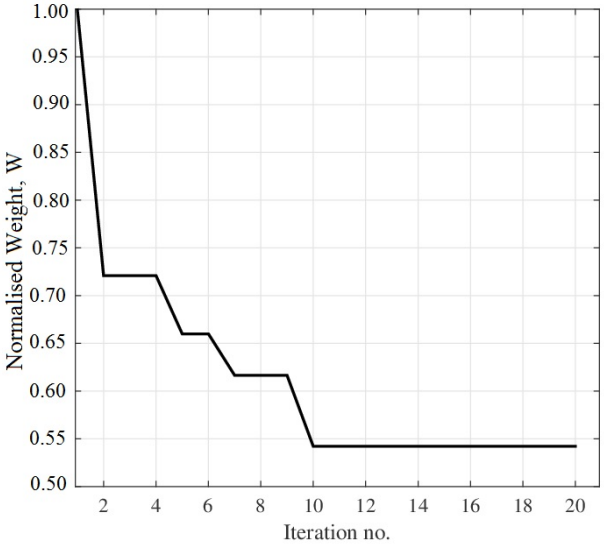

Figure 9: Weight convergence plot for deterministic model.

The buckling analysis results yielded the minimum value for critical load factor of 1.0473 for the first ten buckling modes which is close to the requirement specified for the optimisation problem.

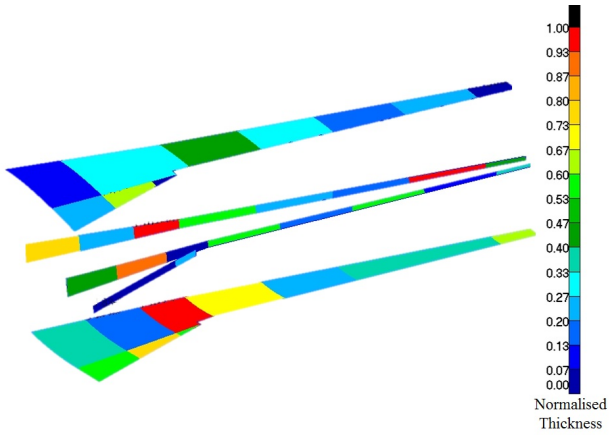

Figure 10: Thickness variation of skin and spar section for deterministic model.

Optimum flutter speed and root bending moments (RBM) for different weighting values are given in Table 4 and the Pareto Optimal Curve are plotted as shown in Fig.12. Note that the values presented here is the normalised value against the highest observed value. As expected, the optimal flutter speed is obtained when a higher weighting value is specified ($w_f = 0.9$) and vice-versa, the minimum RBM value is obtained at a higher weighting value for gust at $w_g = 0.9$. A weighting factor was applied for both flutter and gust responses in order to evaluate the contribution of the response to optimal results. The ideal flutter speed and root bending moment response is 0.5029 and 0.5719, respectively. Here, the average principle was applied where the sum of ratio of the

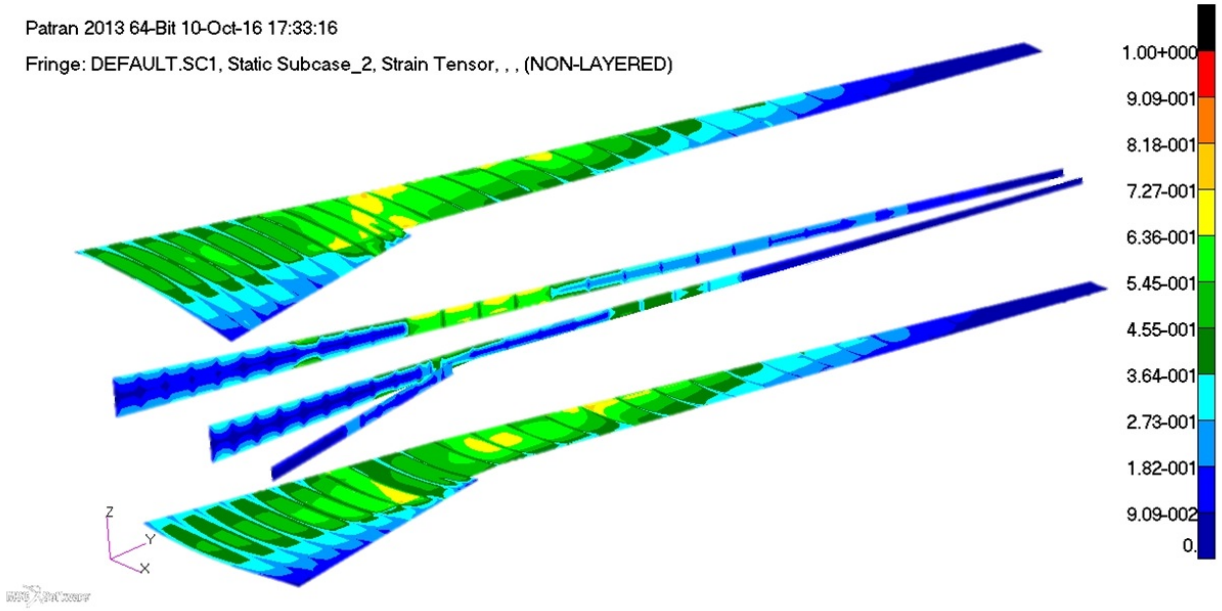

Figure 11: Normalised strain distribution of the wing structure for optimum deterministic model.

flutter speed to the design flutter speed ($1.15V_D$) and the minimum RBM value to the RBM value should be close to 2 for the ideal case.

Table 4: Deterministic optimisation results for flutter speed, V_f and wing root bending moment, RBM.

Weighting		Response (normalised)	
w_f	w_g	V_f	RBM
1.0	0.0	0.5013	3.4411
0.9	0.1	0.5005	2.6653
0.8	0.2	0.5005	1.4092
0.7	0.3	0.5228	1.4121
0.6	0.4	0.5025	0.8535
0.5	0.5	0.5051	0.9112
0.4	0.6	0.5119	1.0226
0.3	0.7	0.5012	0.6978
0.2	0.8	0.5029	0.5719
0.1	0.9	0.6828	0.4162
0.0	1.0	0.8294	0.4884

5.3. Robust optimisation

The deterministic and robust optima for the three layup strategies at normalised design flutter speed of 0.6667 and normalised design wing root bending moment of 0.6429 are presented in Table 5, along with the mean, standard deviation and probability of failure for the design values. Figs. 13, 14 and 15 compare the Probability Density Function (PDF) for the flutter speed and RBM of the deterministic optima as well as robust optima evaluated at design flutter speed and design RBM values.

The mean value for the flutter speed for all layup strategies are higher compared to the ideal flutter speed obtained from the deterministic model due to the variation in the longitudinal, E_1, transverse in-plane Young's modulus, E_2 and ply thickness in the model. The probability of failure at flutter design speed for deterministic flutter response increases as extra design space is introduced. With all layup strategies, the robust optimisation result is considerably more reliable design with lower probabilities of failure compared to the deterministic solution.

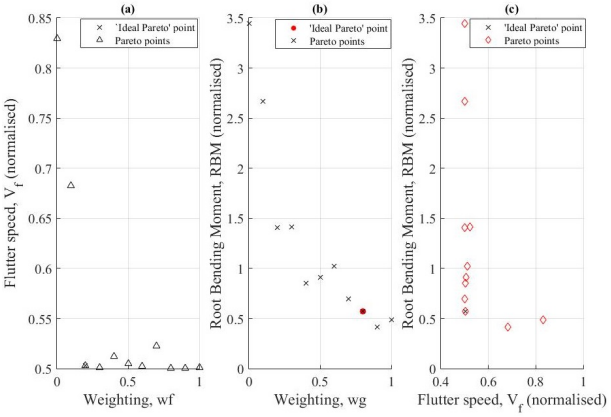

Figure 12: Deterministic optimisation results: (a) Flutter speed at different weighting function, w_f plot, (b) RBM values at different weighting function, w_g plot and (c) Flutter speed against RBM value plot

A 32.6% reduction in terms of the probability of failure is achieved over the laminate with only 0°,

Table 5: Robust optimisation results for 1) 0°, ±45° and 90°, 2) 0°, ±30°, ±45°, ±60° and 90° and 3) 0°, ±15°, ±30°, ±45°, ±60°, ±75° and 90° plies.

Layup Stategy	Objective	Flutter speed, V_f (normalised) ($V_{f,\text{Design}} = 0.6667$)			Root Bending Moment, RBM (normalised) ($RBM_{\text{Design}} = 0.6429$)		
		Mean	Std Dev.	Probability of failure	Mean	Std Dev.	Probability of failure
1	Deterministic	0.6179	0.1643	0.008900	0.7499	0.1166	0.0023
	Robust	0.7126	0.1028	0.006000	0.6991	0.1238	0.0135
2	Deterministic	0.7117	0.0760	0.009600	0.6193	0.1209	0.4641
	Robust	0.7105	0.0866	0.000529	0.3622	0.1052	1.0000
3	Deterministic	0.6856	0.1829	0.031900	0.5202	0.1177	0.9851
	Robust	0.7196	0.0752	0.017700	0.3789	0.1359	1.0000

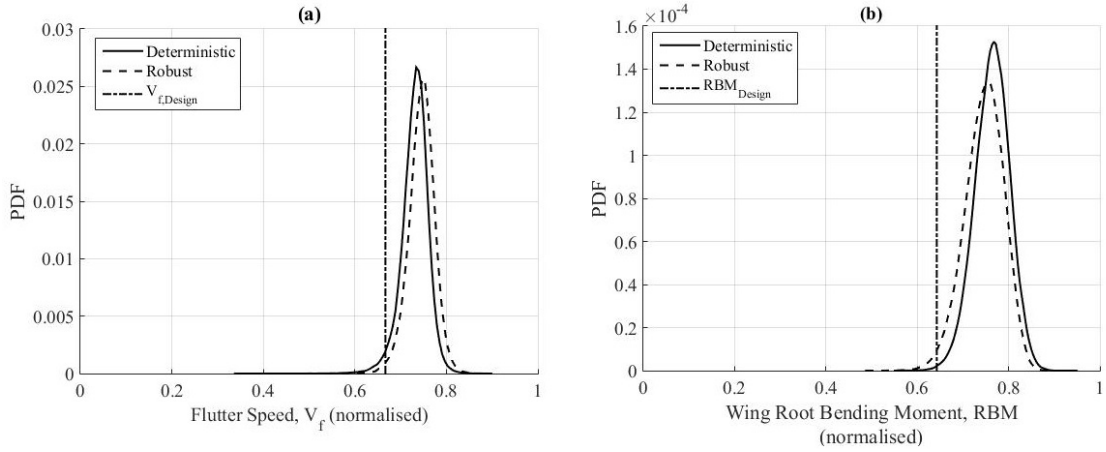

Figure 13: Comparison PDFs for deterministic and robust design with 0°, ±45° and 90° plies: (a) Flutter response (b) RBM response.

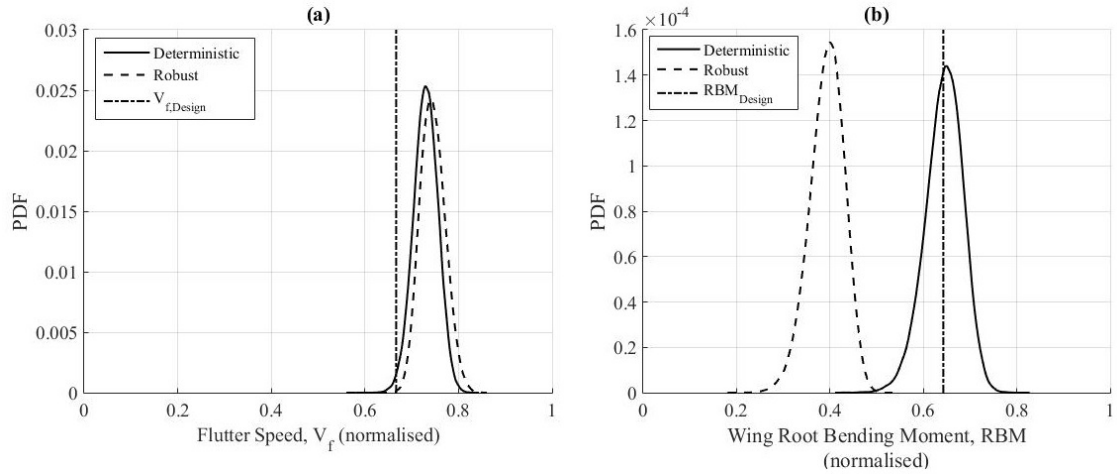

Figure 14: Comparison PDFs for deterministic and robust design with 0°, ±30°, ±45°, ±60° and 90° plies: (a) Flutter response (b) RBM response.

±45° and 90° plies. Higher percentage of reductions in terms of probability of failure are achieved with the inclusion of additional plies with 94.6% and 44.8% reductions obtained for second and third layup strategy, respectively.

For the gust responses, the mean values for root bending moment are reduced for all layup strategies with the highest reduction of 41.5% obtained with the inclusion of ±30° and ±60° plies. Figs. 14(b) and 15(b) show that the PDF curves are shifted to the left

to accommodate for minimum value of RBM. Only small improvements in terms of the RBM probability of failure are achieved for the first layup strategy due to limited design spaces. It is noteworthy that the PDF curve for robust flutter response using the third layup strategy as shown in Fig. 15(a) is shifted to the left and has a higher peak probability value as compared to the deterministic solution. However, it also noticed that the skewness of the deterministic PDF curve is reduced for the robust design and thereby lowering the probability of failure at design flutter speed.

Finally, it can be remarked that the inclusion of extra design space in terms of the ply angles provide improvement in reliability resulting in higher flutter speed and lower RBM. The layup strategy with 0°, ±30°, ±45°, ±60° and 90° plies give the optimal robust solution for both flutter and root bending responses. Fig. 16 shows the ply configuration for optimal robust solution with second layup strategy of $[\theta_1\theta_2...\theta_n]_s$ where, n is the ply number.

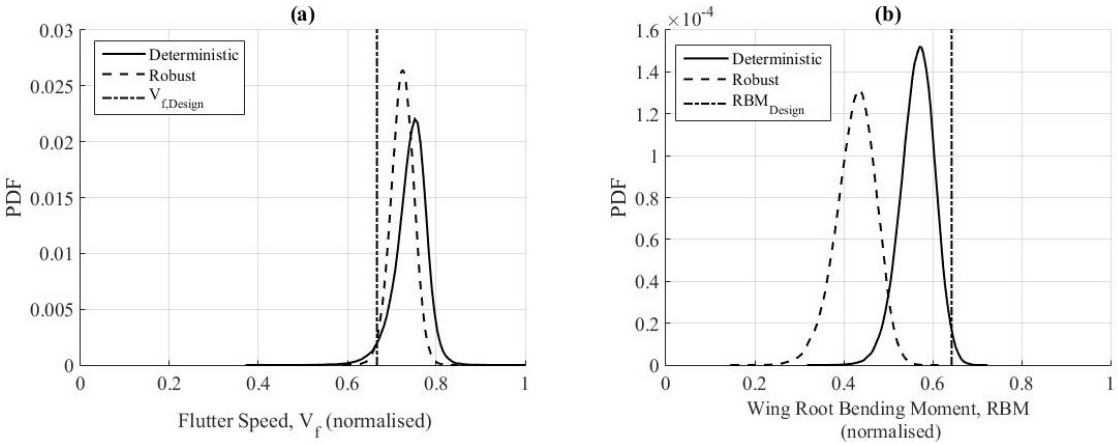

Figure 15: Comparison PDFs for deterministic and robust design with 0°, ±15°, ±30°, ±45°, ±60°, ±75° and 90° plies: (a) Flutter response (b) RBM response.

		PLY NO.																												
	PANEL NO.	1	2	3	4	5	6	7	8	9	10	11	12	13	14	15	16	17	18	19	20	21	22	23	24	25	26	27	28	29	30
TOP SKIN 1	1	45	90	-30	30	90	-60	90	90																						
	2	45	0	30	90	-30	30	60	-60	90	-60	-60	90																		
	3	45	0	-30	0	60	45	-60	90	-60	-60	-60	90	90																	
	4	45	0	0	45	0	45	60	60	-60	30	-60	60	-60	60	60	90														
	5	45	0	30	30	30	60	90	90	-45	-60	90	90	-60																	
	6	45	0	0	-60	90	90	90	-60	60	90																				
	7	45	0	30	-45	30	90	90	90	90	-60	90																			
	8	45	0	90	-60	90																									
TOP SKIN 2	9	45	0	30	30	-60	90	90	90	-60	90	-60																			
	10	45	0	30	30	0	30	30	0	45	90	60	30	90	30	45	60	45	45	-30	30	60	90								
	11	45	90	90	0	-60	90																								
BOTTOM SKIN 1	1	45	30	30	60	0	-60	30	90	-45	-30	90	-60	60	90																
	2	45	0	30	-45	90	90	60	90	-60	90																				
	3	45	90	0	30	30	45	0	30	30	0	-60	30	45	0	30	30	30	0	0	-30	0	30	0	0	0	0	90	30	-30	30
	4	45	0	30	30	60	0	0	0	60	30	90	45	45	30	-45	30	60	45	-30	30	60	60	30							
	5	45	30	0	45	90	-30	90	-60	90	90	-60																			
	6	45	0	0	30	30	30	90	60	60	-60	-60	60	-60	60	90															
	7	45	0	0	30	30	30	60	60	90	60	90	90	-60	90	-60															
	8	45	0	30	30	0	90	45	30	0	30	45	30	30	30	60	90	-45	60	60	-60	60									
BOTTOM SKIN 2	9	45	0	30	30	0	0	90	45	-60	30	45	30	-30	60	30	-60	60	90	60	90										
	10	45	30	30	0	90	30	0	0	30	45	30	30	0	45	60	0	30	60	-60	60	-60	30	0	-30	-60					
	11	45	30	0	30	0	30	0	90	30	45	-60	60	45	90	60	60	45	60	-60											
SPAR 1	1	45	30	0	30	0	30	30	0	45	30	90	30	90	45	90	30	30	90	-30	60	60	0	90	-30						
	2	45	0	30	-60	-45	90	30	90	-60	90	90																			
	3	45	0	30	30	30	0	45	30	60	30	0	90	0	30	30	-45	90	0	90	0	45	0	60	60	-30	60	30	90	30	-60
	4	45	0	0	30	30	30	60	0	45	30	60	-60	90	-60	90	-60	0	60	-60	90										
	5	45	-30	0	90	-45	30	60	90	90	-60	90																			
	6	45	0	-30	45	90	60	90	-60	90	90																				
	7	45	0	30	0	30	30	0	30	30	0	45	-60	30	90	90	30	-60	-60	60	45	90	30	-45	60	-60	0	30	0	30	-60
	8	45	0	30	0	-45	0	90	45	60	45	45	60	60	-60	-30	90	60													
SPAR 2	1	45	30	30	0	60	60	0	60	60	30	-45	60	-45	90	45	-60														
	2	45	60	30	0	0	30	0	30	60	30	90	0	30	30	-45	30	0	45	30	0	30	30	90	-45	30	60	90	0		
	3	45	0	90	90	-60	90																								
	4	45	0	30	30	0	90	30	30	30	30	-45	30	30	90	-60	90	60	90	60	45										
	5	45	45	-30	0	90	-60	90	90	-60	90																				
	6	45	0	0	30	30	60	0	30	30	60	45	90	45	45	90	-60	-60	-60	30	90										
	7	45	-60	0	-60	90	60	90	90																						
	8	45	0	30	30	45	0	45	-60	90	90	90	-45	60	90	60															
SPAR 3	1	45	-60	0	90	90																									
	2	45	0	90	90	-60																									
	3	45	-30	90	30	30	-30	-60	90	90	-60	90																			

Figure 16: Ply configuration for robust design configuration with 0°, ±30°, ±45°, ±60°, and 90° plies.

6. Conclusion

A computationally efficient approach has been presented for the robust design of composite wings with multiple constraints and uncertain material properties, ply orientations and ply thicknesses. Polynomial Chaos Expansion is used as a stochastic model for the uncertainties quantification to estimate the Probability Density Function (PDF) and probability of failure for aeroelastic and gust responses. The robust design configuration has been achieved based on minimum probability of failure for flutter response and minimum mean value for RBM response which is obtained from optimisation using the Particle Swarm Optimisation algorithm. Three layup strategies were undertaken, a first which only consists of 0°, ±45° and 90° plies, a second which also included ±30° and ±60° plies and a third which also uses ±15° and ±75° plies. The following observations have been made:

- The optimal normalised weight of 0.8866 is obtained for a deterministic optima design which is a 11.3% reduction from the baseline design.
- Polynomial Chaos Expansion (PCE) provides sufficient accuracy for uncertainties quantification with fewer model runs (order of two magnitude reduction) compared to Monte Carlo Simulation.
- A minimum improvement in reliability of 32.6% is achieved for a laminate with 0°, ±45° and 90° plies for flutter response and highest reduction in mean RBM value is obtained with the inclusion of ±30° and ±60° plies.
- The layup strategy with 0°, ±30°, ±45°, ±60° and 90° plies gives the optimal robust solution for both flutter and root bending moment responses.

It is also noted that the thickness variation obtained from the optima deterministic solution has not considered manufacturing constraints, such as composite ply drops, which may provide more beneficial results for robust design which are subject to future work.

Acknowledgements

The authors would like to acknowledge the support of the EPSRC, who provide funding for the ACCIS Centre for Doctoral Training Centre (EP/G036772/1), Embraer S.A. and also the Ministry of Higher Education, Malaysia and University Sains Malaysia for the scholarship.

References

[1] M. H. Shirk, T. J. Hertz, T. Weisshaar, Aeroelastic tailoring — theory, practice, and promise, Journal of Aircraft 23 (1) (1986) 6–18.

[2] F. E. Eastep, V. A. Tischler, V. B. Venkayya, N. S. Khot, Aeroelastic Tailoring of Composite Structures, Journal of Aircraft 36 (6) (1999) 1041–1047.

[3] S. Kuzmina, V. Chedrik, F. Ishmuratov, Strength and aeroelastic structural optimization of aircraft lifting surfaces using two-level approach, 6th World Congress of Structural and Multidisciplinary Optimization.

[4] S. Guo, D. Li, Y. Liu, Multi-objective optimization of a composite wing subject to strength and aeroelastic constraints, Proceedings of the Institution of Mechanical Engineers, Part G: Journal of Aerospace Engineering 226 (9) (2011) 1095–1106.

[5] J. Dillinger, T. Klimmek, M. Abdalla, Z. Gürdal, Stiffness optimization of composite wings with aeroelastic constraints, Journal of Aircraft.

[6] M. Y. Harmin, J. E. Cooper, Aeroelastic Tailoring Using Ant Colony Optimization, 50th AIAA/ASME/ASCE/AHS/ASC Structures, Structural Dynamics and Materials Conference, 4-7 May (May) (2009) 1–17.

[7] O. Stodieck, J. E. Cooper, P. M. Weaver, P. Kealy, Improved aeroelastic tailoring using tow-steered composites, Composite Structures 106 (2013) 703–715.

[8] Z. Wan, B. Zhang, Z. Du, C. Yang, Aeroelastic two-level optimization for preliminary design of wing structures considering robust constraints, Chinese Journal of Aeronautics 27 (2) (2014) 259–265.

[9] N. P. M. Werter, R. D. Breuker, Aeroelastic Tailoring and Structural Optimisation using an Advanced Dynamic Aeroelastic Framework, International Forum on Aeroelasticity and Structural Dynamics (2015) 1–20.

[10] I. de Visser, Aeroelastic and strength optimization of a composite aircraft wing using a multilevel approach, Proceedings of the 40 th Structures, Structural Dynamics, and Materials Conference and Exhibit, 1999.

[11] E. L. Walker, T. K. W. Iv, Integrated Uncertainty Quantification for Risk and Resource Management : Building Confidence in Design (Invited), 53rd AIAA Aerospace Sciences Meeting, AIAA SciTech (January) (2015) 1–17.

[12] E. Livne, Future of Airplane Aeroelasticity, Journal of Aircraft 40 (6) (2003) 1066–1092.

[13] C. Scarth, J. E. Cooper, P. M. Weaver, G. H. Silva, Uncertainty quantification of aeroelastic stability of composite plate wings using lamination parameters, Composite Structures 116 (2014) 84–93.

[14] A. Manan, J. Cooper, Uncertainty of Composite Wing Aeroelastic Behaviour, 12th AIAA/ISSMO Multidisciplinary Analysis and Optimization Conference.

[15] E. P. Wiser, Monte Carlo Technique with Correlated Random Variables 118 (2) (1992) 258–272.

[16] T.-U. Kim, I. H. Hwang, Optimal design of composite wing subjected to gust loads, Computers & Structures 83 (19-20) (2005) 1546–1554.

[17] G. Georgiou, A. Manan, J. Cooper, Modeling composite wing aeroelastic behavior with uncertain damage severity and material properties, Mechanical Systems and Signal Processing 32 (2012) 32–43.

[18] D. Xiu, G. Em Karniadakis, Modeling uncertainty in steady state diffusion problems via generalized polynomial chaos, Computer Methods in Applied Mechanics and Engineering 191 (43) (2002) 4927–4948.

[19] S. Sarkar, J. A. S. Witteveen, A. Loeven, H. Bijl, Effect of uncertainty on the bifurcation behavior of pitching airfoil stall flutter, Journal of Fluids and Structures 25 (2) (2009) 304–320.

[20] S. C. Castravete, R. A. Ibrahim, Effect of Stiffness Uncertainties on the Flutter of a Cantilever Wing, AIAA Journal 46 (4) (2008) 925–935.

[21] H. T. Hahn, S. W. Tsai, Introduction to Composite Materials, Taylor & Francis, 1980.

[22] M. Kameyama, H. Fukunaga, Optimum design of composite plate wings for aeroelastic characteristics using lamination parameters, Computers and Structures 85 (2007) 213–224.

[23] K. Marlett, Hexcel 8552 IM7 Unidirectional Prepreg 190 gsm & 35%RC Qualification Material Property Data Report (2011) 238.

[24] E. H. Johnson, MSC Nastran Version 68 Aeroelastic Analysis User's Guide - 2, Structure.

[25] S. S. Rao, Optimization of airplane wing structures under taxiing loads, Computers and Structures 26 (3) (1987) 469–479.

[26] S. S. Rao, L. Majumder, Optimization of Aircraft Wings for Gust Loads: Interval Analysis-Based Approach, AIAA Journal 46 (3) (2008) 723–732.

[27] EASA, Certification Specifications for Large Aeroplanes, Cs-25 (September) (2008) 750.

[28] MSC Software Corporation, MSC Nastran 2012 Dynamic Analysis User's Guide, 2011.

[29] D. Xiu, G. E. Karniadakis, The Wiener–Askey Polynomial Chaos for Stochastic Differential Equations, SIAM Journal on Scientific Computing 24 (2) (2002) 619–644.

[30] S.-K. Choi, R. V. Grandhi, R. A. Canfield, C. L. Pettit, Polynomial Chaos Expansion with Latin Hypercube Sampling for Estimating Response Variability, AIAA Journal 42 (6) (2004) 1191–1198.